Corrosion inhibition of carbon steel in saline water using an azo dye at various concentrations

R.A. Mohammed* and S.Z. Hussein

Department of Chemistry, Collage of Science, University of Baghdad, Jadriyah, Baghdad, 10011, Iraq
**E-mail: rawaa.a.mohammed@sc.uobaghdad.edu.iq*

Abstract

Potentiodynamic measurements were used to examine the corrosion-inhibiting impact of 4-[6-bromo-benzothiazolylazo]thymol (BTAT) on low carbon steel (LCS) in 3.5% NaCl solution at various temperatures (293–323 K) and concentrations. It was discovered that with increasing concentration of BTAT dye, the inhibition efficiency (*IE*%) increased up to 94.6%. Additionally, the results indicated that as the temperature increases, the inhibition efficiency diminishes. As the inhibitor concentration is increased to 70 ppm, the corrosion rate decreases. By calculating the temperature dependence of corrosion rate derived from Tafel plots, the effective activation energy was determined both in the absence and in the presence of various concentrations of BTAT dye. Atomic force microscopy (AFM) was utilized for characterizing the morphological properties of the metal surface before and after addition of the dye. Moreover, the dye revealed antibacterial ability against gram positive (*Staphylococcus aureus*) and gram negative bacteria (*Escherichia coli*).

Received: December 16, 2023. Published: February 2, 2024 doi: 10.17675/2305-6894-2024-13-1-12

Keywords: *4-[6-bromobenzothiazolylazo]thymol (BTAT), low carbon steel (LCS), electrochemical measurements, azo dye, inhibitors, corrosion.*

1. Introduction

Corrosion can be defined as an electrochemical process that combines two coupled reactions, namely, anodic ionization of the metal and cathodic process of reduction of the oxidizing agent-depolarizer, each of which occurs at the expense of the other. Numerous works have been conducted to increase the durability of structures and materials. In fact, corrosion is one of the primary issues in these works [1–3]. Steel corrosion can be defined as one of the primary corrosion issues in various sectors since steel is less expensive than other materials and is used more frequently. In general, carbon steel is the most commonly utilized type of steel [4, 5]. The amount of carbon in carbon steel majorly determines its characteristics. The carbon content of the majority of carbon steels is much lower than 1%. Many goods, such as kitchen appliances, cans, structural beams, and car bodies are manufactured of carbon steel [6–10]. One of the methods for controlling this type of corrosion involves the use of organic inhibitors [11, 12]. Inhibitors are compounds whose small amounts stop or lessen the

corrosion reactions [13, 14]. Inhibitors adsorb on the metal surface, thus reducing the corrosion rate. Compounds which contain π bonds are thought to be the most efficient inhibitors [15–17]. The electronic structures of inhibiting molecules, steric factor, aromaticity, and electron density at the donor site, molecular area, and molecular weight of the inhibitor are factors that affect the adsorption of such compounds on the steel surface [18]. It is important to emphasize that compounds with functional groups, such as CO, CHO, R–OH, and N=N, act as efficient corrosion inhibitors [19–21]. The most adaptable category of dyes is azo colorings [22]. Numerous spectral data studies have previously been published, and their structure was the subject of extensive study [23, 24]. The most common applications for the dyes were in the areas of advanced organic synthesis, textile dyeing, medicinal research, and high-tech industries such as liquid crystal displays, lasers, inkjet printers, and electro-optical devices [25]. Moreover, azo dyes possess a broad spectrum of unique biological applications, good dyeing and sensing properties [26]. Various dyes' adsorption characteristics have been documented [26, 27]. One azo dye that was utilized in the study of azo derivatives as well as their chemical behavior is 4-[6-bromobenzothiazolylazo]thymol (BTAT), which has the chemical formula $C_{17}H_{13}N_3SOBr$ (MW: 387 g/mol). BTAT dye's chemical structure is depicted in Figure 1. Previously, the dye was created by reacting 6-bromo-2-aminobenzothiazole with nitrous acid in a diazotization reaction [28]. This study's primary goal is to determine how much the BTAT dye inhibits the growth of LCS in 3.5% NaCl solution at various concentrations and temperatures (293, 303, 313, and 323 K) using the potentiodynamic polarization technique.

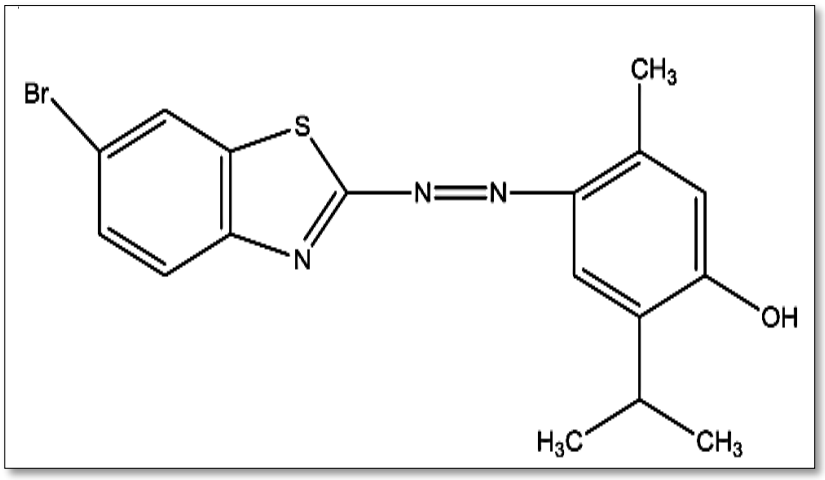

Figure 1. Chemical structure of BTAT mono azo dye.

2. Experimental

2.1. Solution

The corrosive solution contained 3.50% sodium chloride (NaCl, 99.5%, BDH company (*Supplier*) and the BTAT dye with concentrations of 30, 50, and 70 ppm as the inhibitor.

2.2. Specimens and polarization curves

The measurement was carried out using the Bank Elek's three electrode potentiostatic system (Mlab200 model). Silver/silver chloride served as the reference electrode, platinum rods served as the counter electrode, and round pieces of LCS alloy measuring 2.5 cm×0.2 mm were used as the working electrode. The LCS specimens had the following composition (mass%): Mn 0.199, Fe 99.5, C 0.0855, Si <0.0100, Cu 0.0260, Ni <0.0250, Cr 0.0341, Al 0.0441, and other metals (0.096). A working electrode of LCS was polished using SiC emery papers ranging in grade from 400 to 1200. The polished samples were then cleaned in ethanol (C_2H_5OH, 99.9%, BDH), dried in the air, and cleaned with distilled water prior to being immersed in the corrosive solution.

2.3. Antibacterial activity

The antibacterial activity of the dye was studied against two bacteria strains: gram positive (*Staphylococcus aureus*) and gram negative (*Escherichia coli*). The well diffusion method was used to evaluate the *in vitro* antibacterial activity [29]. Briefly, petri dishes were prepared with about 25 mL of autoclaved nutritional agar placed onto sterile plates. Then, the plates were allowed to solidify, after which 18 hours grown [OD adjusted to 0.6] 100 μL of above-mentioned pathogenic bacteria was transferred onto the plate and a culture lawn was made with an L-rod spreader that was sterile. After 5 min setting of the pathogenic microbes, a sterile cork borer was used to make a 6 mm well on the prepared plates (agar). The dye was dissolved in sterile water and loaded into wells (50 μL/well). The solvent sterile water, which served as the negative control, and azithromycin (30 μL/well), which served as the positive control, were loaded into the wells. Then, the plates were incubated at 37°C for 24 hours in an incubator to determine the zone of inhibition. The inhibition zone was measured in mm [30, 31]. In addition, the inhibition zone calculations were made according to the Clinical and Laboratory Standards Institute, as follow: weak antibacterial activity (<10 mm), moderate antibacterial activity (10–13 mm) and strong antibacterial activity (>13 mm) [31].

3. Results and Discussion

3.1. Corrosion rate measurements

The electrochemical corrosion kinetics of any system could be described through measuring 3 polarization parameters: Tafel slopes (cathodic (β_c) and anodic (β_a)), corrosion current density (i_{corr}), and corrosion potential (E_{corr}), from a polarization curve (*E vs*. *i*). The corrosion rate is calculated by evaluating these factors, and it is frequently converted to the Faradaic corrosion rate, which has units of (mm/y). Tafel parameters include corrosion current density (i_{corr}), corrosion potential (E_{corr}), and the slopes β_c and β_a. The corrosion inhibitory abilities related to the LCS samples in saline water (3.5% NaCl) media have been assessed from Tafel extrapolation plots as well as evaluated with blank ones. The impact of an increase in

concentration up to 70 ppm on the corrosion rate was examined. The relation that uses Eq. 1 to determine the inhibition efficiency (*IE*%) is as follows [32, 33]:

$$IE\% = \left[1 - \frac{i_{corr}}{i_{corr}^{0}}\right] \cdot 100 \quad (1)$$

In which cathodic Tafel lines' extrapolation to corrosion potential yields corrosion current densities related to the blank as well as inhibited specimens, respectively, denoted by the values i_{corr} and i_{corr}^{0}. Figure 2 displays the potentiodynamic polarization curves regarding the LCS specimens under examination, both without and with inhibitors, immersed in a 3.5% NaCl solution at 293–313 K.

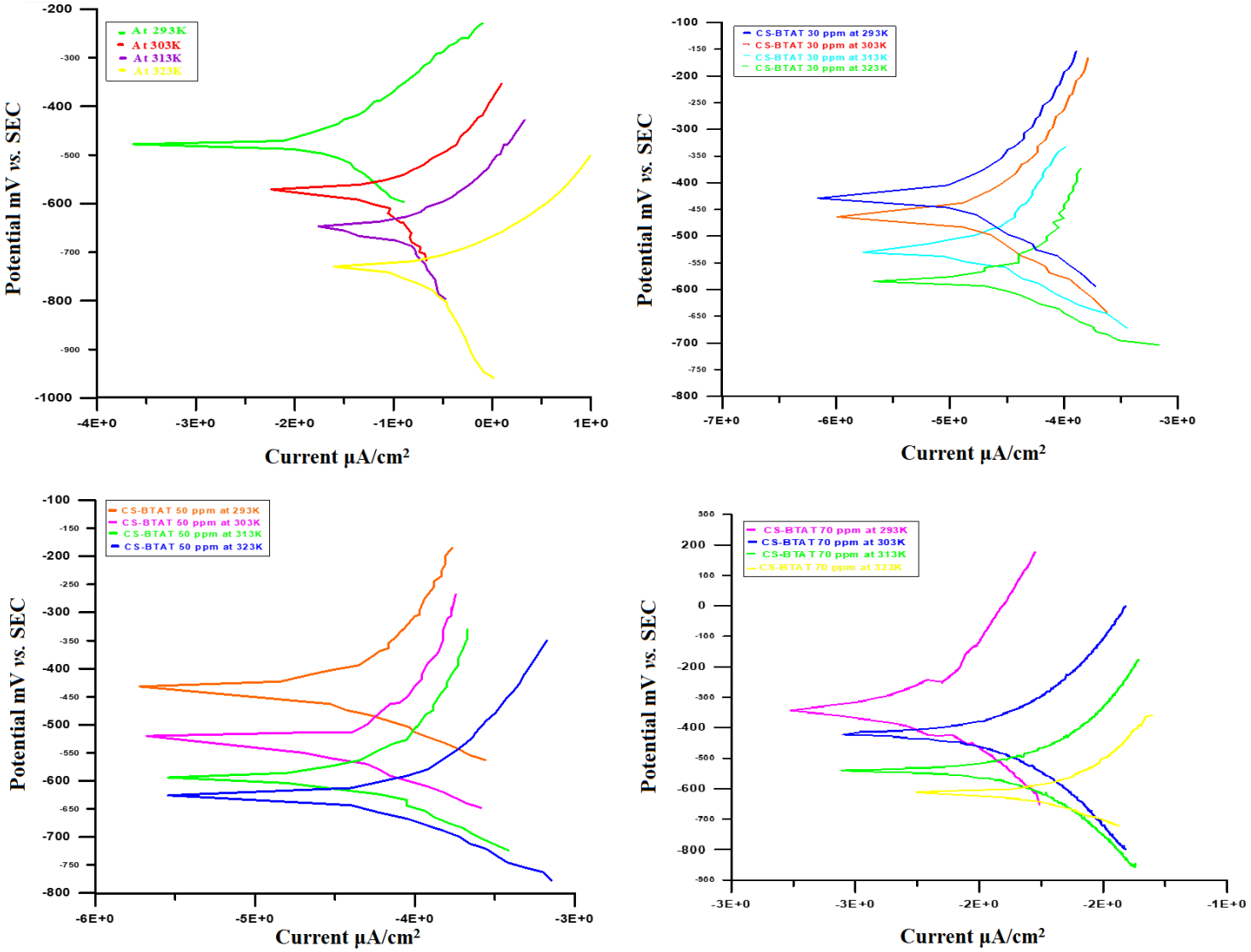

Figure 2. Potentiodynamic polarization curves for the LCS in the absence and in the presence of various concentrations of BTAT dye at 293–313 K.

Table 1 illustrates how E_{corr} in the LCS–BTAT system shifts to a more positive potential (noble direction) when compared to blank sample, indicating the inhibitor's ability to hinder corrosion. It demonstrates that the values related to the corrosion current density (i_{corr}) for LCS–BTAT are lower compared to those for blank LCS, wherein i_{corr} decreases as the BTAT concentration in the 3.5% NaCl solution increases. Nonetheless, as temperatures rise, (i_{corr}) rises as well. The most significant examined parameter is the inhibitor's *IE*%, which shows how the inhibition affects the sample. At 70 ppm, LCS metal has been shown to be protected most considerably. As the temperature rises, *IE*% falls. This suggests that the inhibition is hindered with a rise in temperature, with the lowest temperature producing the best inhibition efficiency. The considerable reduction in the inhibitor's adsorption on the metal surface as well as the increase in reaction rate that follows are thought to be the causes of *IE*% fall with temperature [34]. Because it contains hydroxyl groups, nitrogen, aromatic rings, and sulfur atoms which combine with metal to form a complex which adsorbs on the surface of alloys and shields them from the corrosive environments, this dye has the best inhibitory efficiency [35].

Table 1. Corrosion parameters acquired from LCS polarization with different concentration levels of BTAT dye at (293–313 K).

	T(K)	E_{corr} (mV)	i_{corr} (μA/cm^2)	β_c (mV/Dec)	β_a (mV/Dec)	*IE*%
Blank LCS	293	–471.8	24.1	–136.4	130.7	
	303	–572.1	79.7	–162.6	132.7	
	313	–646.5	111.3	–186.7	148.5	
	323	–676.8	133.2	–193.9	131.6	
LCS-BTAT/ 30 ppm	293	–426.8	4.9	–139.8	150.0	79.6
	303	–466.2	17.1	–119.3	165.6	78.5
	313	–527.8	25.7	–151.9	147.0	76.9
	323	–580.1	32.9	–97.8	108.4	75.3
LCS-BTAT/ 50 ppm	293	–433.7	2.9	–86.7	118.3	88.0
	303	–528.9	10.3	–122.6	120.2	87.1
	313	–588.7	15.5	130.6	134.3	86.1
	323	–627.3	19.7	–114.8	148.6	85.2
LCS-BTAT/ 70 ppm	293	–325.0	1.3	–119.8	110.6	94.6
	303	–524.8	7.2	–268.5	276.8	91.0
	313	–601.9	12.8	–239.6	260.7	88.5
	323	–610.3	19.9	–228.3	262.7	85.1

3.3. Effect of Temperature

The following formula based on the Arrhenius equation was utilized to investigate how temperature affected the inhibited corrosion reaction of LCS [36–38]:

$$\log i_{corr} = \log A - E_a / 2.303RT \quad (2)$$

in which A represent the pre-exponential factor (in molecules $cm^{-2}s^{-1}$), T represents the temperature (K), R represents the gas constant, and E_a represents the activation energy of the corrosion reaction ($kJ \cdot mol^{-1}$). The values of E_a were determined from the slopes of the linear relationships of ($\log i_{corr}$) *versus* ($1/T$), (Figure 3), while (A) was obtained from the intercept. The following is how the transition state equation is expressed [39, 40]:

$$\log \frac{i_{corr}}{T} = \log\left(\frac{R}{Nh}\right) + \frac{\Delta S^*}{2.303R} - \frac{\Delta H^*}{2.303RT} \quad (3)$$

In which ΔH^* represent the activation enthalpy and ΔS^* represent the activation entropy. The plots of $\log(i_{corr}/T)$ *vs.* $1/T$ displayed in Figure 4 allow entropy change of activation (ΔS^*) and the enthalpy change of activation (ΔH^*) to be calculated from the intercepts and slopes, respectively.

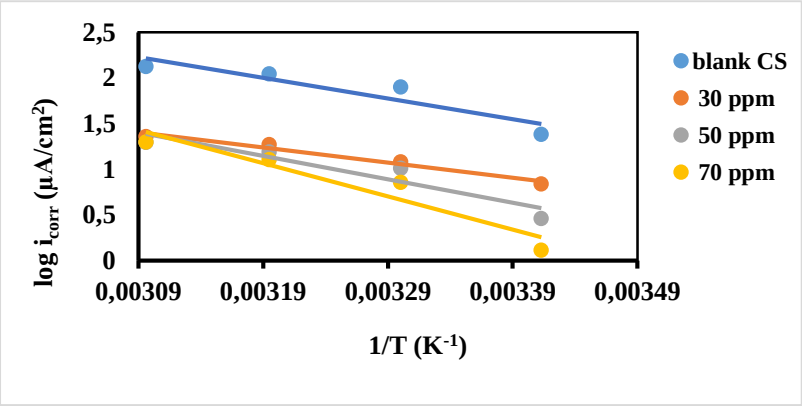

Figure 3. Plots of $\log i_{corr}$ *vs.* $1/T$ for blank and different concentrations of BTAT dye.

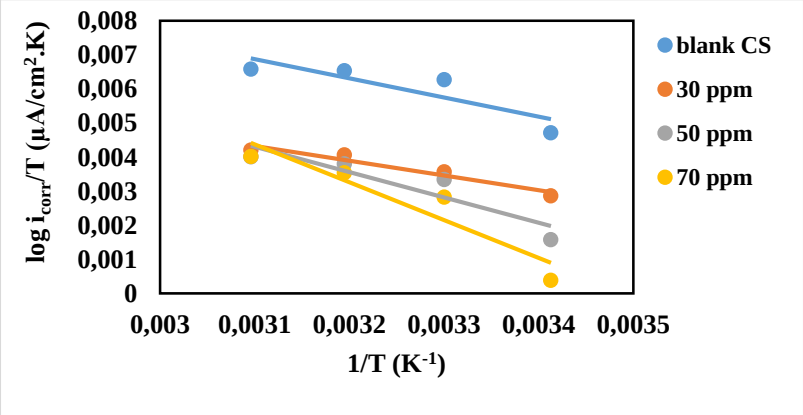

Figure 4. Plot of $\log(i_{corr}/T)$ *vs.* $1/T$ for blank and various concentrations of BTAT dye.

Table 2. Activation parameters for corrosion of blank and inhibited solutions at various inhibitor concentrations in the (293–323) K temperature range.

System	T (K)	E_a (effective) (kJ/mol)	A (molecules·cm^{-2} s^{-1})	ΔH^* (kJ/mol)	ΔS^* (J/mol·K)
Blank LCS	293	43.5	$1.768 \cdot 10^9$	1.10	–197.11
	303				
	313				
	323				
30 ppm	293	45.3	$3.602 \cdot 10^9$	1.29	–197.05
	303				
	313				
	323				
50 ppm	293	48.9	$6.321 \cdot 10^9$	1.46	–197.02
	303				
	313				
	323				
70 ppm	293	69.6	$4.508 \cdot 10^{12}$	2.11	–196.84
	303				
	313				
	323				

According to Table 2, the endothermic nature of steel dissolution process is shown by the positive sign of the activation enthalpy (ΔH^*) [6]. With regard to the tested solution, ΔS^* is negative. An increase in ΔS^* is typically understood as an increase in the disorder that occurs upon transition from reactants to activated complex [41]. E_a values that have been acquired with the inhibitor present are greater than those acquired without it, suggesting a strong inhibitive action for compounds under study through raising the energy barrier with regard to corrosion and highlighting the electrostatic nature regarding inhibitor's adsorption on carbon steel surface [42, 43]. This kind of inhibitor effectively slows down corrosion at room temperature, yet exhibits poorer inhibition at higher temperatures. According to the Arrhenius law, the temperature can affect A and E_a as well as the corrosion rate, which increases with temperature (Eq. 2). According to the values acquired, E_a and A appear to increase steadily as the inhibitor concentration rises [43]. The rise in the energy barrier of the corrosion reaction accounts for the increase in ΔH^* and E_a that goes in parallel with the increase in the inhibitor concentration. The suggested physisorption mechanism is additionally supported by the inhibitor's increased activation energy. Higher values of E_a

indicate a physical adsorption mechanism, whereas lower or unchanged levels of E_a in inhibited systems relative to the blank suggest a chemisorption mechanism [43].

3.4. Atomic Force Microscopy (AFM)

A surface study was carried out to assess the metal's surface state after contact with the corrosive media. AFM images demonstrated the alterations which occur with low carbon steel's surface protection and corrosion. The polished LCS surface related to polishing scratches is shown in Figure 5a prior to exposure to the corrosive solution. Because of the metal dissolution in the corrosive solution, Figure 5b illustrates how badly the LCS surface was harmed when the inhibitor is not there. In contrast, Figure 5c illustrates how much better the surface condition was when the inhibitor was present. The steel's dissolution rate was significantly decreased by forming a good protective layer due to adsorption of inhibitor molecules on the metal surface which are responsible for corrosion inhibition [44–48].

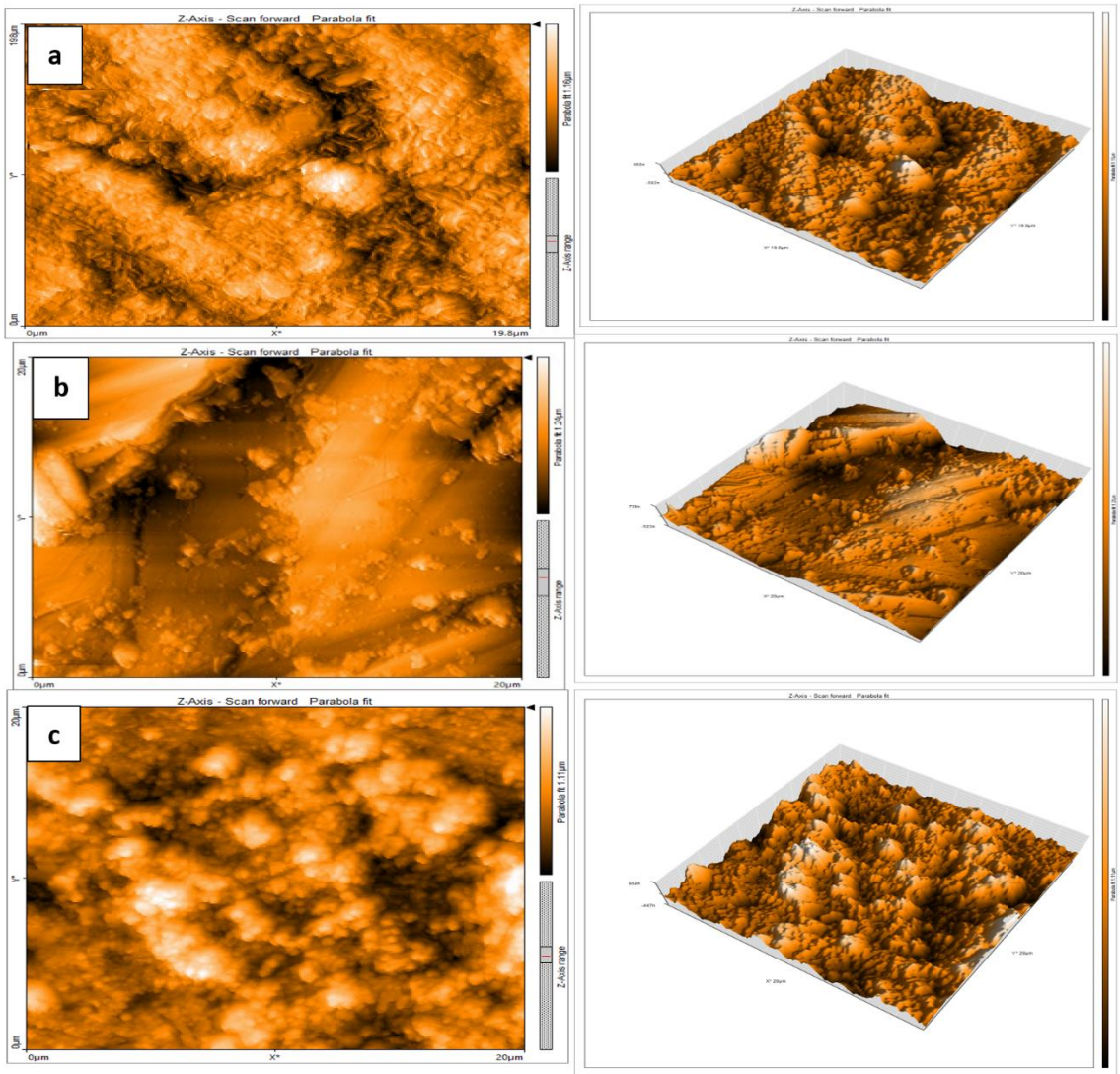

Figure 5. AFM images (2D, 3D) for (a) blank LCS, (b) LCS before adding inhibitor, and (c) LCS after adding inhibitor.

3.5. Antibacterial activity

In this study, the antibacterial activity of the dye was evaluated against two bacterial strains *Escherichia coli* (*E. coli*) and *Staphylococcus aureus* (*S. aureus*). Table 3 lists the effect of the dye in terms of the diameter of the inhibition zone on the bacterial. The dye demonstrated higher antibacterial activity against gram negative bacteria (*E. coli*) compared to gram positive bacteria *(S. aureus*). Therefore, gram negative bacteria were shown to be more vulnerable than gram positive bacteria by the dye's antibacterial action. According to Salamou *et al*., the azo (–N=N–) chromophore in the molecule is what would be responsible for the azo compound's increased antibacterial activity [49]. Moreover, the azo compounds work by hydrophobic, hydrogen bonding, and halogen interactions, which increase their binding strength to the enzymes' active sites present on bacterial membranes [50].

Table 3. The inhibition zones for antibacterial activity.

Microorganism strains	Inhibition zone (mm)
E. coli	15
S. aureus	13

Conclusion

The following is a summary of the current work's findings:

1. LCS is significantly inhibited by BTAT dye.
2. The optimal concentration is determined to be 70 ppm, where the highest efficiency of 94.6% is achieved.
3. The efficacy of inhibitor's ability to inhibit corrosion rose as its concentration rose and fell as the temperature rose.
4. The fact that the corrosion potential moved in the positive direction with increasing inhibitor concentration indicates that this dye functions as an anodic inhibitor.
5. As the inhibitor concentration rises, the corrosion rate decreases.
6. As the concentration of inhibitors decreases, the current density increases.
7. From AFM analyses, the BTAT inhibitor established a protective system for the metal.
8. The dye exhibited a high antibacterial effect against gram negative and gram positive bacteria.

References

1. P. Thiraviyam and K. Kannan, A study of synthesized Mannich base inhibition on mild steel corrosion in acid medium, *J. Iran. Chem. Soc*., 2012, **9**, 911–921. doi: 10.1007/s13738-012-0108-1
2. N.O. Eddy, F. Awe and E.E. Ebenso, Adsorption and inhibitive properties of ethanol extracts of leaves of *Solanum melongena* for the corrosion of mild steel in 0.1 M HCl, *Int. J. Electrochem. Sci*., 2010, **5**, 1996–2011. doi: 10.1016/S1452-3981(23)15401-0

3. H.H. Kadhim and K.A. Saleh, Removing of Copper ions from Industrial Wastewater Using Graphene oxide/Chitosan Nanocomposite, *Iraqi J. Sci*., 2022, 1894–1908. doi: 10.24996/ijs.2022.63.5.4
4. M.H. Raheema, N.A. Khudhair, T.H. AL-Noor, S.R. Al-Ayash, H.H. Kharnoob and S.M. Obed, Enhancement of corrosion protection of metal carbon steel C45 and stainless steel 316 by using inhibitor (Schiff base) in sea water, *Baghdad Sci. J*., 2023, **20**, 1012–1012. doi: 10.21123/bsj.2023.7749
5. R.M. Kubba, M.M. Kazem, S.M. Al-Majidi and A.A.-K.M. Ali, Experimental Studies for Carbon Steel Corrosion Inhibition in 3.5% NaCl Solution by Two New N-Benzyl-5-Bromo Isatin Derivatives, *Int. J. Appl. Innov. Eng. & Manage*., 2016, **5**, 28–43.
6. S. Eid and W.M. Hassan, Chemical and theoretical studies for corrosion inhibition of magnesium in hydrochloric acid by tween 80 surfactant, *Int. J. Electrochem. Sci*., 2015, **10**, 8017–8027. doi: 10.1016/S1452-3981(23)11073-X
7. M. Abdallah, E. Kamar, S. Eid and A. El-Etre, Animal glue as green inhibitor for corrosion of aluminum and aluminum-silicon alloys in sodium hydroxide solutions, *J. Mol. Liq*., 2016, **220**, 755–761. doi: 10.1016/j.molliq.2016.04.062
8. R.T. Salim and D.E. AL-Mammar, Adsorption of Azo Dye Onto TiO_2 Nanoparticles Prepared by a Novel Green Method: Isotherm and Thermodynamic Study, Iraqi Journal of Science, 2023, pp. 4679-4692. DOI: 10.24996/ijs.2023.64.8.5.
9. R. A. Mohammed and K. A. Saleh, Electropolymerization of [N-(1,3-thiazo-2-yl)] maleamic acid and their Nanocomposite with Graphene Oxide as Protective Coating against Corrosion and Antibacterial Action, *Iraqi J. Sci*., 2022, 4163–4174. doi: 10.24996/ijs.2022.63.10.3
10. M.T. Mohammed, W.N. Al-Sieadi and O.H. Al-jeilawi, Corrosion inhibitor of carbon steel in 3.5% NaCl solution with Schiff base compounds, *Int. J. Health Sci*., 2022, **6**, 57–75. doi: 10.53730/ijhs.v6nS6.9172
11. K.D. Demadis, C. Mantzaridis and P. Lykoudis, Effects of structural differences on metallic corrosion inhibition by metal − polyphosphonate thin films, *Ind. Eng. Chem. Res*., 2006, **45**, 7795–7800. doi: 10.1021/ie0607898
12. I.M. Al-mousawi, R.S. Ahmed, N.J. Kadhim and A.M. Farhan, Study of Corrosion Inhibition for Mild Steel in Hydrochloric Acid Solution by a new furan derivative, *J. Phys.: Conf. Ser*., 2021, 022061. doi: 10.1088/1742-6596/1879/2/022061
13. R.A. Mohammed and D.E. Al-Mammar, Using tobacco leaves as adsorbent for the orange-G dye removal from its aqueous solutions, *J. Global Pharma Technol*., 2019, **11**, 273–280.
14. A.A. Mizhir, H.S. Al-Lami and A.A. Abdulwahid, Kinetic, Isotherm, and Thermodynamic Study of Bismarck Brown Dye Adsorption onto Graphene Oxide and Graphene Oxide-Grafted-Poly (*n*-butyl methacrylate-co-methacrylic Acid), *Baghdad Sci. J*., 2022, **19**, 0132. doi: 10.21123/bsj.2022.19.1.0132

15. K.D. Alanazi, B.H. Alshammari, T.Y. Alanazi, O.A. Alshammari, A.M. Ashmawy, M.M. Aljohani, R. Abdel Hameed and A.M. Deyab, Green Synthesis of a Novel Cationic Surfactant Based on an Azo Schiff Compound for Use as a Carbon Steel Anticorrosion Agent, *ACS Omega*, 2023, **8**, no. 51, 49009–49016. doi: 10.1021/acsomega.3c06710
16. Z.I. Jasim, K.H. Rashid, K.F. AL-Azawi and A.A. Khadom, Synthesis of Schiff-Based Derivative as a Novel Corrosion Inhibitor for Mild Steel in 1 M HCl Solution: Optimization, Experimental, and Theoretical Investigations, *J. Bio- Tribo-Corros*., 2023, **9**, 54. doi: 10.1007/s40735-023-00774-5
17. M.B. Hamza and E.I. Yousif, New Metal Complexes Derived from Azo Linked Schiff-Base ligand: Synthesis, Spectral Investigation and Biological Evaluation, *J. Univ. Anbar Pure Sci*., 2023, **17**, no. 2, 154–164. doi: 10.37652/juaps.2023.142314.1108
18. Z.T. Khudhair and M.S. Shihab, Study of Some Azo Derivatives as Corrosion Inhibitors for Mild Steel in 1 M H_2SO_4, *Surf. Eng. Appl. Electrochem*., 2022, **58**, 708–719. doi: 10.3103/S1068375522060151
19. J. Aljourani, K. Raeissi and M. Golozar, Benzimidazole and its derivatives as corrosion inhibitors for mild steel in 1M HCl solution, *Corros. Sci*., 2009, **51**, 1836–1843. doi: 10.1016/j.corsci.2009.05.011
20. M. Attia, K. Soliman, S. Eid and E. Mabrouk, Experimental and theoretical study on some azo chromotropic acid dyes compounds as inhibitor for carbon steel corrosion in sulfuric acid, *J. Iran. Chem. Soc*., 2022, **19**, 655–664. doi: 10.1007/s13738-021-02329-2
21. S.H. Kareem and A. Enaas, Adsorption of Congo, Red Rhodamine B and Disperse blue dyes from aqueous solution onto raw flint clay, *Baghdad Sci. J*., 2012, **9**, 680–688.
22. N.H. AL-Shammari and D.E. AL-Mammar, Adsorption of Biebrich Scarlet Dye into Remains Chromium and Vegetable Tanned Leather as Adsorbents, *Iraqi J. Sci*., 2022, **63**, no. 7, 2814–2826. doi: 10.24996/ijs.2022.63.7.6
23. T.J. Greenfield, M.M. Turnbull, J. Zubieta and R.P. Doyle, Synthesis and structural and magnetic characterization of an Iron(III) pyrophosphate complex with 1,10′-phenanthroline, *Inorg. Chim. Acta*, 2019, **498**, 119084. doi: 10.1016/j.ica.2019.119084
24. A.M. Abdullah and A.A.S. Al-Hamdani, Synthesis, Characterization, Thermal Studies and Antioxidant Activities of Transition Metal Complexes with Azo Dye ligand, *Baghdad Sci. J*., 2023. doi: 10.21123/bsj.2023.8365
25. K. Serbest, T. Dural, M. Emirik, A. Zengin and Ö. Faiz, Heteroligand bivalent transition metal complexes with an azo-oxime ligand and 1,10-phenanthroline: Synthesis, spectroscopy, thermal analysis, DFT calculations and SOD-mimetic activities, *J. Mol. Struct*., 2021, **1229**, 129579. doi: 10.1016/j.molstruc.2020.129579
26. E.E. El-Katori, R.A. El-Saeed and M.M. Abdou, Anti-corrosion and anti-microbial evaluation of novel water-soluble bis azo pyrazole derivative for carbon steel pipelines in petroleum industries by experimental and theoretical studies, *Arabian J. Chem*., 2022, **15**, 104373. doi: 10.1016/j.arabjc.2022.104373

27. H.M. Al-Saidi, G.A. Gouda, M. Abdel-Hakim, N.I. Alsenani, A. Alfarsi, M.H. Mahross, O.A. Farghaly and Sh. Hosny, Synthesis and characterization of Ni(II), Cu(II), Zn(II) and Azo dye based on 1,10-*o*-phenanthroline binary complexes: Corrosion inhibition properties and computational studies, *Int. J. Electrochem. Sci*., 2022, **17**, 220333. doi: 10.20964/2022.03.45
28. A.K. Abaas, D.E. Al-Mammar and H.A. Abbas, Equilibrium, Thermodynamic and Kinetic Study of the Adsorption of a New Mono Azo dye onto Natural Iraq Clay, *J. Global Pharma Technol*., 2018, **10**, no. 5, 102–109.
29. F. Al-Khikani and A. Ayit, The Antibacterial Action of Safranin and Gentian Violet, *Rambam Maimonides Med. J*., 2022, **13**, no. 3, e0018. doi: 10.5041/RMMJ.10475
30. T. Akshaya, M. Aravind, S. Manoj Kumar and B. Divya, Evaluation of *In-vitro* antibacterial activity against gram-negative bacteria using silver nanoparticles synthesized from *Dypsis lutescens* leaf extract, *J. Chil. Chem. Soc*., 2022, **67**, 5477–5483. doi: 10.4067/S0717-97072022000205477
31. R. Londonkar and M. Kesralikar, *In Vitro* Anticancer Screening of Methanolic Extract of *Stachytarpheta Mutabilis*, *Proceedings of the conference BioSangam 2022: Emerging trends in Biotechnology (BIOSANGAM 2022)*, 2022, 188–204. doi: 10.2991/978-94-6463-020-6_19.
32. B. Xue, Y. Jiang and D. Liu, Preparation and characterization of a novel anticorrosion material: Cu/LLDPE nanocomposites, *Mater. Trans*., 2011, **52**, 96–101. doi: 10.2320/matertrans.M2010280
33. R.W. Revie, Uhlig's corrosion handbook, John Wiley & Sons, 2011, 51. doi: 10.1002/9780470872864
34. E. Mabrouk, S. Eid and M. Attia, Corrosion inhibition of carbon steel in acidic medium using azo chromotropic acid dye compound, *J. Basic Environ. Sci*., 2017, **4**, 351–355.
35. A. Al-Sarawy, A. Fouda and W.S. El-Dein, Some thiazole derivatives as corrosion inhibitors for carbon steel in acidic medium, *Desalination*, 2008, **229**, 279–293. doi: 10.1016/j.desal.2007.09.013
36. M. Hegazy and M. Zaky, Inhibition effect of novel nonionic surfactants on the corrosion of carbon steel in acidic medium, *Corros. Sci*., 2010, **52**, no. 4, 1333–1341. doi: 10.1016/j.corsci.2009.11.043
37. E. Abd Dleam and S.H. Kareem, Mesoporous silica nanoparticles as a system for ciprofloxacin drug delivery; kinetic of adsorption and releasing, *Baghdad Sci. J*., 2021, **18**, 0357–0357. doi: 10.21123/bsj.2021.18.2.0357
38. H.R. Ali, S.S. Hassan and N.J. Kadhim, Preparation & Characterization of Complexes Containing Beta Lactam & Study of the Effect of Corrosion Inhibition Using Iron Resistant Stainless Steel, *Pak. J. Med. Health Sci*., 2022, **16**, 589–589. doi: 10.53350/pjmhs22168589
39. F. Al-Nowaiser, M. Abdallah and E. El-Mossalamy, N,N-di(polyoxyethylene)-4-dodecylaniline as a corrosion inhibitor for steel in hydrochloric acid solutions, Chemistry and technology of fuels and oils, 2012, **47**, 453–463. doi: 10.1007/s10553-012-0324-5

40. A.M. Alqudsi and K.A. Saleh, Conducting Polyanethole/Metals Oxides Nanocomposites for Corrosion Protection and Bioactivity, *Baghdad Sci. J.*, 2023. doi: 10.21123/bsj.2023.8458
41. M. Elachouri, M. Hajji, M. Salem, S. Kertit, J. Aride, R. Coudert and E. Essassi, Some nonionic surfactants as inhibitors of the corrosion of iron in acid chloride solutions, *Corrosion*, 1996, **52**, 103–108. doi: 10.5006/1.3292100
42. Z.-Y. Liu, D. Wang, D.-T. Li and H.-Q. Wang, The inhibition efficiencies of some organic corrosion inhibitors of iron: An insight from density functional theory study, *Comput. Theor. Chem*., 2022, **1214**, 113759. doi: 10.1016/j.comptc.2022.113759
43. I. El Ouali, B. Hammouti, A. Aouniti, Y. Ramli, M. Azougagh, E. Essassi and M. Bouachrine, Thermodynamic characterisation of steel corrosion in HCl in the presence of 2-phenylthieno(3,2-b) quinoxaline, *J. Mater. Environ. Sci*., 2010, **1**, 1–8.
44. P. Vennila, S. Kavitha, G. Venkatesh and P. Madhu, Experimental and theoretical investigation of *Rosmarinus officinalis* leaves extracts as the corrosion inhibitor for mild steel in H_3PO_4 solution; synergistic effect, *Pharma Chem*., 2015, **7**, 275–283.
45. X. Li, S. Deng, H. Fu and X. Xie, Synergistic inhibition effects of bamboo leaf extract/major components and iodide ion on the corrosion of steel in H_3PO_4 solution, *Corros. Sci*., 2014, **78**, 29–42. doi: 10.1016/j.corsci.2013.08.025
46. Z.Z. Almarbd and N.M. Abbass, Synthesis and characterization of TiO_2, Ag_2O, and graphene oxide nanoparticles with polystyrene as a nanocomposites and some of their applications, *Eurasian Chem. Commun*., 2022, **4**, 1033–1043. doi: 10.22034/ecc.2022.342801.1469
47. R.M. Kubba and M.A. Mohammed, Theoretical and Experimental Study of Corrosion Behavior of Carbon Steel Surface in 3.5% NaCl and 0.5 M HCl with Different Concentrations of Quinolin-2-One Derivative, *Baghdad Sci. J*., 2022, **19**, 0105. doi: 10.21123/bsj.2022.19.1.0105
48. H.H. Kadhim and K.A. Saleh, Removing Cobalt ions from Industrial Wastewater Using Chitosan, *Iraqi J. Sci*., 2022, **63**, no. 8, 3251–3263. doi: 10.24996/ijs.2022.63.8.1
49. N.A. Salamou, T. Jean-de-Dieu, S.F. Emmanuel, M.T. Germaine, B.M.T. Gabin, P.F. Simon, A. Tsopmo and K. Jules-Roger, Synthesis, characterization, and antibacterial activity of a new poly azo compound containing N-arylsuccinimid and dibenzobarrelene moieties, *Heterocycl. Commun*., 2023, **29**, 20220157. doi: 10.1515/hc-2022-0157
50. M. Di Martino, L. Sessa, M. Di Matteo, B. Panunzi, S. Piotto and S. Concilio, Azobenzene as Antimicrobial Molecules, *Molecules*, 2022, **27**, 5643. doi: 10.3390/molecules27175643

♦ ♦ ♦